Thermochemical and Structural Stability of A- and B-Site-Substituted Perovskites in Hydrogen-Containing Atmosphere

Elena Konysheva* and John T. S. Irvine

School of Chemistry, University of St Andrews, St Andrews, Fife, KY 16 9ST, U.K.

Received November 4, 2008. Revised Manuscript Received February 10, 2009

The thermochemical and structural stability of complex perovskites $A_{1-x}A'_xB_{1-y-z}B'_yB''_zO_{3\pm\delta}$ (A, A′ = La, Sr and B, B′, B″ = Ni, Mn, Fe, Co) was explored in H_2-Ar atmosphere (5% H_2−95% Ar) in a wide temperature range by thermogravimetric analysis, differential thermal analysis, XRD, and HRTEM. All perovskites showed good thermochemical stability in a temperature range of 25−300 °C. Reduction of the perovskites occurs at temperatures higher than 300 °C and can be interpreted as a multistep process. At the initial stage of exposure to H_2-Ar, a small weight gain was observed. This might indicate direct sorption of hydrogen into the lattice, forming hydride−oxide phases. On the other hand, the oxide lattice could reduce to form water, and then, the evolved water is reincorporated into the lattice to give a small weight gain. This is followed by dramatic weight loss. Water was found to be the main gaseous product formed during reduction. Complex perovskites, depending upon composition, rapidly lose up to 6−12 mol % of the lattice oxygen, which is accompanied by phase or structural transformations in the solid. Further mechanism and kinetics of reduction strongly depend on temperature. The rate of reduction at intermediate temperatures (500−700 °C) becomes slow, probably due to a local stabilization of $La(OH)_3$ in extremely humidified hydrogen-containing atmosphere. The complete reduction of perovskites can occur at 800 °C. On long-term annealing, the perovskite containing three transition elements and Sr on the B and A sublattices, respectively, showed better thermochemical stability in hydrogen-containing atmosphere. The results suggest that the presence of structural defects and their mobility in the oxygen sublattice are important factors determining the thermochemical stability of perovskites.

1. Introduction

Perovskite-related materials with transition metals in high formal oxidation states are important as catalysts, superconductors, battery materials, electronic ceramics, and electrodes for fuel cells. The use of perovskites with promising properties, however, is very often limited by their stability under reducing condition.

The thermochemical stability of $LaBO_3$ perovskites containing one transition element on the B sublattice (B = Cr, Mn, Fe, Co, Ni) was explored earlier at high temperature (1000 °C and 1 atm).[1] It was shown that they have good thermochemical stability in air. This fact is in agreement with the high values of their crystal field stabilization energy.[2] The values of the tolerance factor evaluated for these perovskites (eq 1)[3] are close to 1, indicating good structural stability.[2]

$$t = \frac{d_{A-O}}{d_{B-O}\sqrt{2}} \quad (1)$$

Here d_{A-O} and d_{B-O}represent the average distances (in Å). $LaNiO_{3-\delta}$ is the only exception, which decomposes in air at high temperature.[4] The thermochemical stability of $LaBO_3$ perovskites (B = Cr, Mn, Fe, Co, Ni) was found to decrease at low oxygen partial pressure in the following sequence[1]

$$LaCrO_3>LaFeO_3>LaMnO_3>LaCoO_{3.01}>LaNiO_{2.99} \quad (2)$$

Notice that the first three compositions (Cr-, Fe-, or Mn-containing perovskites) exhibit orthorhombic structure, whereas the last two compositions (Co and Ni containing perovskites) display rhombohedral structure. Partial substitution of La^{3+} for Sr^{2+} on the A sublattice raises simultaneously the oxygen vacancy concentration and the fraction of transition cations on the B sublattice in the highest oxidation state, thereby strongly influencing the thermochemical stability and transport properties of $A_{1-x}A'_xBO_{3\pm\delta}$ perovskites.[5,6] Further works demonstrated that the thermochemical stability of $AB_{1-y}B'_yO_{3\pm\delta}$ perovskites could be further improved through the substitution on the B sublattice by transition metals.[7,8] Nevertheless, the thermochemical stability of perovskites containing more than one cation on the A and B sublattices has not been investigated widely at intermediate tempera-

* Corresponding author. Tel: +44-1334-463844. Fax: +44-1334-463808. E-mail: ek31@st-andrews.ac.uk.

(1) Nakamura, T.; Petzow, G.; Gauckler, L. J. *Mater. Res. Bul.* **1979**, *14*, 649.
(2) Yokokawa, H. *Annu. Rev. Mater. Res.* **2003**, *33*, 581.
(3) Goldschmidt, V. M. *Naturwissenschaften* **1926**, *14*, 477.
(4) Drennan, J.; Travares, C. P.; Steele, B. C. H. *Mater. Res. Bull.* **1982**, *17*, 621.
(5) Nitadori, T.; Misono, M. *J. Catal.* **1985**, *93*, 459.
(6) Chan, K. S.; Ma, J.; Jaenicke, S.; Chuah, G. K.; Lee, J. Y. *Appl. Catal., A* **1994**, *107*, 201.
(7) Chiba, R.; Yoshimura, F.; Sakurai, Y. *Solid State Ionics* **1999**, *124*, 281.
(8) Falcon, H.; Baranda, J.; Campos-Martin, J. M.; Pena, M. A.; Fierro, J. L. G. *Stud. Surf. Sci. Catal.* **2000**, *130*, 2195.

10.1021/cm802996p CCC: $40.75
Published on Web 03/19/2009

tures. Most published results illustrate defect structure of perovskites, oxygen stoichiometry, transport properties, and their electrocatalytic activity with respect to oxygen reduction.[9−12] The number of publications describing the thermochemical stability under reducing conditions is quite limited, and they rarely demonstrate the mechanism and kinetics of reduction and phase/structural transformations in perovskites at high and intermediate temperatures.[10,13−15] Thermodynamic data for evaluation of the Gibbs free energy of formation of $A_{1-x}A'_xB_{1-y}B'_yO_{3\pm\delta}$ perovskite compounds in the certain circumstances (in particular under low oxygen partial pressure) often are not available or the evaluation procedure is very sophisticated.[16]

Therefore, in the present work, the thermochemical and structural stability of A- and B-site-substituted complex perovskites $La_{1-x}Sr_xMn_{1-y-z}Ni_yFe_zO_{3\pm\delta}$ was studied in hydrogen-containing atmospheres in a wide temperature range (25−800 °C). In addition, at certain stages the thermochemical stability of A-site-substituted $LaBO_3$ perovskites ($La_{0.8}Sr_{0.2}MnO_{3\pm\delta}$ and $La_{0.6}Sr_{0.4}CoO_{3\pm\delta}$) was studied to consider in more detail the mechanism and kinetics of reduction.

2. Experimental Section

2.1. Sample Preparation. Initial perovskite compositions $La_{0.95}Ni_{0.6}Fe_{0.4}O_{3-\delta}$ (LNF), $La_{0.8}Sr_{0.2}MnO_{3\pm\delta}$ (LSM), and $La_{0.6}Sr_{0.4}CoO_{3\pm\delta}$ (LSC) were produced by combustion spray pyrolysis and supplied by PRAXAIR Inc. (Danbury, CT). The initial compositions have a purity of 99.9%. The compositions $La_{0.935}Sr_{0.02}Ni_{0.54}Fe_{0.36}Mn_{0.1}O_{3-\delta}$ (LSMNF90), $La_{0.92}Sr_{0.04}Ni_{0.48}Fe_{0.32}Mn_{0.2}O_{3-\delta}$ (LSMNF80), and $La_{0.872}Sr_{0.104}Ni_{0.288}Fe_{0.192}Mn_{0.52}O_{3\pm\delta}$ (LSMNF48) were obtained by mechanical mixing of LNF and LSM perovskites, followed by calcination in air at 1350 °C for 5 h. Initial powders (LNF, LSM, and LSC) and the pellet made of LNF (93% final density) and LSC (92% final density) were also annealed at the same temperature.

2.2. Characterization Methods. Thermochemical stability was analyzed by thermogravimetric analysis (TGA) on NETZSCH TG 209 and NETZSCH STA 449C instruments (NETZSCH-Geraetebau GmbH, Selb, Germany). Three types of experiments were carried out: thermal cycling (TC), isothermal experiments, and reduction/reoxidation cycle (ROC). The thermal cycling was carried out on powders under H_2−Ar (5% H_2−95% Ar) in a temperature range of 25−800 °C with a heating/cooling rate of 5 °C/min. In the case of the isothermal experiments, a sample was heated up in air to operating temperature (500, 600, 700, or 800 °C) with a rate of 5 °C/min and equilibrated in air up to 1 h. A gas atmosphere was further changed to argon and then to H_2−Ar. The sample was exposed to H_2−Ar for a period up to 10 h, and finally, it was cooled down in the same atmosphere to room temperature at a rate of 50 °C/min. These experiments were carried out on different powders and pellets under different H_2−Ar gas flow rates (6−32 mL/min). In addition, the isothermal experiments with LNF and LSMNF48 powders (only at 800 °C and under H_2−Ar gas flow rate of 15 mL/min) were performed for shorter periods of exposure to H_2−Ar (between 0.2 and 4 h) to study phase and structure transformations in the solid phases. During the reduction/reoxidation cycle (ROC), a sample was heated up in air to 800 °C with a rate of 25 °C/min and equilibrated in air. A gas atmosphere was further changed to argon and H_2−Ar, like in the isothermal experiments. The sample was exposed to H_2−Ar for 0.3 h. The gas atmosphere was changed in turn to argon and then to air. Finally, the sample was cooled down to room temperature at a rate of 50 °C/min. The initial weight of all samples (powders and pellets) was about 60 mg (for all experiments) and about 100 mg (for ROC). In addition, differential thermal analysis (DTA) was conducted simultaneously with TGA on a NETZSCH STA 449 C instrument. The effect of buoyancy was corrected using blank runs with alumina crucibles under corresponding flow rates and gas atmospheres (in the text referred to as "correction"). During TGA−DTA measurements, the composition of gas atmosphere over samples and over an alumina crucible without sample was monitored by means of a Thermostar TM mass spectrometer (Pfeiffer-Vacuum LTD, Newport, UK). All results for TGA and DTA are presented in the text after the subtraction of the corresponding corrections. Original TGA−DTA data for ROC (corrections and original data for samples) are available as Supporting Information. They illustrate the reproducibility of the measurements carried out. The TG balance has a resolution of 1 μg. The sensitivity is 0.7 μV/μW (alumina crucible). H_2−Ar gas used for TGA−DTA measurements was analyzed in the chamber with $P(O_2)$ sensor and contains 0.1−0.2% H_2O.

X-ray powder diffraction (XRD) patterns were recorded at room temperature in transmission mode on a STOE Stadi-P diffractometer with Cu Kα radiation (Stoe & Cie GmbH, Darmstadt, Germany). Si powder (Alfa Aesar, Karlsruhe, Germany) was used as the external standard for the calibration of the diffractometer. The diffraction data were refined by the Rietveld method.[17,18] The microstructure of LNF powder after different periods of exposure to H_2−Ar at 800 °C was analyzed by high-resolution transmission electron microscopy (HRTEM) (JEOL JEM2011, JEOL, Tokyo, Japan). The Brunauer−Emmett−Teller (BET) surface area was measured with nitrogen on an ASAP 2020 Instrument (Micrometrics Instrument Corp., Norcross, GA) and an Intelligent Gravimetric Analyzer (Hiden Analytical Ltd., Warrington, U.K.).

3. Results and Discussion

3.1. Crystal Structure. Details of the crystal structure of the perovskites investigated are summarized in Table 1. LNF, LSMNF90, LSMNF80, LSM, and LSC have rhombohedral structure ($R\bar{3}c$, No. 167), whereas LSMNF48 exhibits orthorhombic structure (*Pbnm*; standard setting *Pnma*, No. 62).[19−23] The values of the tolerance factor (eq 1)[3] are close to 1. The oxygen content per formula unit ($3\pm\delta$) and the average oxidation state (z) of the transition metals on the B sublattice were evaluated from the weight loss of samples during their

(9) Li, S.; Jin, W.; Xu, N.; Shi, J. *J. Mater. Sci.* **2000**, *35*, 4329.
(10) Pena, M. A.; Fierro, J. L. G. *Chem. Rev.* **2001**, *101*, 1981.
(11) Zuev, A.; Singheiser, L.; Hilpert, K. *Solid State Ionics* **2002**, *147*, 1.
(12) Kim, G.; Wang, S.; Jacobson, A. J.; Reimus, L.; Brodersen, P.; Mims, C. A. *J. Mater. Chem.* **2007**, *1*, 7–2500.
(13) Reller, A.; Renner, B.; Becker, O.; Ebbinghaus, S. *Solid-State Chem. Inorg. Mater. III, MRS Proc.* **2000**, *658*, GG4.2.
(14) Alifanti, M.; Auer, R.; Kirchnerova, J.; Thyrion, F.; Grange, P.; Delmon, B. *Appl. Catal., B* **2003**, *41*, 71.
(15) Tao, S.; Irvine, J. T. S.; Plint, S. M. *J. Phys. Chem. B* **2006**, *110*, 21771.
(16) Grundy, A. N.; Hallstedt, B.; Gaucker, L. J. *Solid State Ionics* **2004**, *173*, 17.
(17) Rietveld, H. M. *Acta Crystallogr.* **1967**, *22*, 151.
(18) Rietveld, H. M. *J. Appl. Crystallogr.* **1969**, *2*, 65.
(19) Mamak, M.; Metraux, G. S.; Petrov, S.; Coombs, N.; Ozin, G. A.; Green, M. A. *J. Am. Chem. Soc.* **2003**, *125*, 5161.
(20) Konysheva, E.; Irvine, J. T. S.; Besmehn, A. *Solid State Ionics* **2008**, *179*, 1432.
(21) Konysheva, E.; Irvine, J. T. S. *J. Mater. Chem* **2008**, *18*, 5147.
(22) Falcon, H.; Goeta, A. E.; Punte, G.; Carbonio, R. E. *J. Solid State Chem.* **1997**, *133*, 379.
(23) Sonntag, R.; Neov, S.; Kozhukharov, V.; Neov, D.; ten Elshof, J. E. *Physica B* **1998**, *241−243*, 39.

Table 1. Chemical Composition, Oxygen Content, and Structure of the Compounds Analyzed, as Well as Phase Composition after the Decomposition

composition	structure	tolerance factor, t, (eq 1)	oxygen content per formula unit, $(3 \pm \delta)_{initial}$[a]	average oxidation state of cations into the B sublattice, z	phase composition after the decomposition in H_2-Ar
LSM	$R\bar{3}c$[19]	0.992	2.940 ± 0.005	3.081	La_2O_3, SrO, and MnO
LSMNF48	$Pbnm$[20,21]	0.996	[b]2.958 ± 0.012	3.092	La_2O_3, MnO, SrO, and $FeNi_x$
LNF	$R\bar{3}c$[22]	0.993	2.872 ± 0.005	2.890	La_2O_3 and $FeNi_x$
LSMNF90	$R\bar{3}c$[20,21]	0.993	2.899 ± 0.005	2.953	La_2O_3, SrO, MnO, and $FeNi_x$
LSMNF80	$R\bar{3}c$[20,21]	0.993	2.830 ± 0.005	2.821	La_2O_3, SrO, MnO, and $FeNi_x$
LSC	$R\bar{3}c$[23]	0.997	3.000 ± 0.005	3.40	La_2O_3, SrO, and Co

[a] It was determined from the weight change of samples during their decomposition in H_2-Ar at 800 °C. [b] At 900 °C.

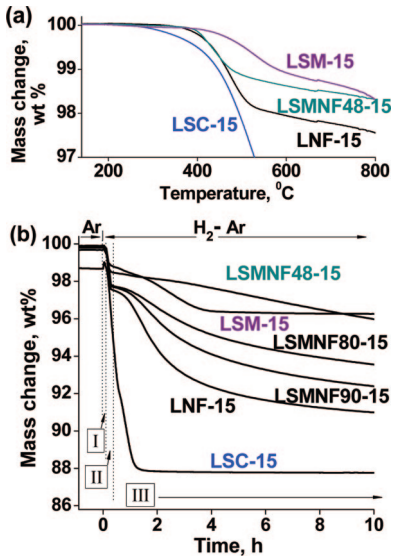

Figure 1. Mass change of perovskites during exposure to H_2-Ar: (a) during thermal cycling with a rate of 5 °C/min and (b) at 800 °C for a period up to 10 h. XXX-15 used in the abbreviation of samples refers to H_2-Ar gas flow rate, which equals to 15 mL/min. The borders between I, II, and III stages are conditionally marked, since they change for different perovskites.

decomposition in H_2-Ar (Table 1). The average oxidation state of cations on the B sublattice of LSMNF48,[21] LSM, and LSC is higher than "3+", unlike for LNF, LSMNF80, and LSMNF90 (Table 1.) It is difficult to interpret the results for LSMNF48, LSMNF80, and LSMNF90, since all transition elements (Mn, Ni, and Fe) are able to change oxidation state simultaneously though the "double exchange mechanism"[24] without variation in oxygen stoichiometry.

3.2. Thermochemical Stability in H_2-Ar. Figure 1a illustrates the thermochemical stability of perovskites in H_2-Ar atmosphere during thermal cycling (TC). LSC started losing weight at a temperature of 300−320 °C, which was lower by about 70−80 °C compared to LNF and LSMNF48 (Figure 1a). Notice that the onset reduction temperature of LNF and LSMNF48 is very close in spite of the difference in the average oxidation state of the B cations, the degree of A-site deficiency, and Sr substitution. It could indicate the involvement of the same type of cations (most probably Ni) in the reduction process at the initial stage. In the case of LSM, the weight loss was observed after about 420 °C and showed slower kinetics. These perovskites, then, underwent isothermal exposure to H_2-Ar at 800 °C in order to study in detail the mechanism and kinetics of reduction (Figure 1b). The weight of the samples changed continuously with time. For the perovskites investigated, one can distinguish three stages. They are marked in Figure 1b accordingly. Stage I is characterized by a slight increase in weight. A sharp weight loss was observed during stage II. All compositions showed completely different trends in the decrease of the weight during stage III.

The ROC was, then, carried out for LSMNF48, LNF, and LSC (Figure 2). The samples were exposed to H_2-Ar for 0.3 h, which comprises the time period for stages I and II. The reproducibility is illustrated for LSC by two independent measurements (sample 1 with correction 1 and sample 2 with correction 2). The weight of LNF and LSMNF48 did not change in air and argon at 800 °C (Figure 2a). However, the weight of LSC slightly decreased during heating up to 800 °C in air, which is accompanied by the change from rhombohedral to cubic symmetry.[23] Weight decreased further during exposure to argon. This is in accord with the previous results.[25] After the stabilization of the sample weight, the gas atmosphere was switched from argon to H_2-Ar. A slight weight gain followed by a strong weight loss was observed for LNF, LSC, and LSMNF48 in H_2-Ar atmosphere within 0.3 h, as had been expected. Surprisingly, several thermal effects were detected in this region (Figure 2c). Then, the gas atmosphere was changed back to argon. During exposure to argon, LSMNF48 regained some of its initial weight, whereas the LNF and LSC were practically unchanged (Figure 2a). After further change of atmosphere to air, all perovskites rapidly restored their weight to the initial values. This was accompanied by exothermic change for all three compositions (Figure 2d). The higher the restored weight, the stronger the thermal effect was. This experiment indicates that LSMNF48 containing manganese cations is less reactive with respect to reduction as compared to LNF and LSC. XRD analysis carried out after reoxidation confirmed that LNF and LSMNF48 perovskites have almost the same XRD patterns as before. For instance, LNF initially had rhombohedral structure, $R\bar{3}c$ [$a = 5.5125$ (11) Å, $c = 13.287(4)$ Å]. After exposure to H_2-Ar for 0.3 h and reoxidation, LNF also showed rhombohedral structure, $R\bar{3}c$ [$a = 5.5156(9)$ Å, $c = 13.2816(20)$ Å], although a and c parameters changed slightly. The same trend was observed for LSMNF48: initially it had orthorhombic symmetry, $Pbnm$ [$a = 5.5240(12)$ Å, $b = 5.4736(12)$ Å, $c = 7.765(2)$ Å]; after ROC it had orthorhombic symmetry, $Pbnm$ [$a = 5.529(3)$ Å, $b = 5.471(3)$ Å, $c = 7.792(7)$ Å]. Due to a fast cooling rate (50 °C/min), LSC retained its cubic structure, which is stable at

(24) Cox, P. A. *Transition Metal Oxides*; Oxford: Clarendon Press; 1995; p 283.

(25) Konysheva, E.; Irvine, J. T. S. *ECS Trans.* **2008**, *13* (26), 115.

a temperature higher than 400 °C.[23] However, the rhombohedral symmetry was observed for LSC if it is cooled down to room temperature at a rate of 5 °C/min.

A TG system coupled with mass spectrometer (TGA−MS) was used to identify composition of the gaseous phase during exposure to H_2−Ar. Water was found to be the main gaseous product. In addition, a small amount of atomic oxygen, as well as traces of CO and CO_2, was observed. Figure 2b qualitatively illustrates hydrogen consumption over LNF powder and over an alumina crucible without sample (correction) during ROC. After the introduction of H_2−Ar atmosphere into the chamber with LNF powder, the hydrogen concentration in the gaseous phase increases much more slowly compared to the correction run with an empty alumina crucible, indicating hydrogen uptake.

Oxygen content in perovskites at a certain period of exposure to H_2−Ar can be represented by the value of the oxygen content per formula unit $[(3 \pm \delta)_t]$, and the average oxidation state (z_t) of cations into the B sublattice can be also evaluated:

$$(3 \pm \delta)_t = \frac{M_O/M \times 100\% - \Delta W}{M_O/M \times 100\%}(3 \pm \delta)_{initial} \quad (3)$$

$$z_t = -\frac{(3 \pm \delta)_t z_{O^{2-}} + (1 - x) z_{La^{3+}} + x z_{Sr^{2+}}}{m} \quad (4)$$

M_O and M are the molar weight of oxygen atoms in perovskite and the molar weight of perovskite; ΔW is the weight loss of perovskite during reduction (in wt %); $z_{O^{2-}}$, $z_{La^{3+}}$, and $z_{Sr^{2+}}$ are the charge of O^{2-}, La^{3+}, and Sr^{2+} ions; $(1 - x)$ and x are the concentration of the corresponding cations in the A sublattice; and m is the total concentration of transition cations in the B sublattice. In the present study, the weight loss (in wt %) directly measured in TGA experiments, the oxygen content per formula unit $[(3 \pm \delta)_t]$, and the average oxidation state (z_t) of cations in the B sublattice will be used for analysis and discussion of the results. Stages I and II will be discussed further for all perovskites investigated; stage III will be considered in more detail for LNF and LSMNF48.

3.2.1. Stage I: Sorption of Hydrogen and Formation of H_2O. An increase in the weight at 800 °C was observed for all perovskites powders tested under H_2−Ar gas flow rate of 15 mL/min or lower (Figures 1b and 2a,c and Table 2). The weight gain observed for LSC was significant, whereas it was much lower for LSM, LNF, LSMNF80, and

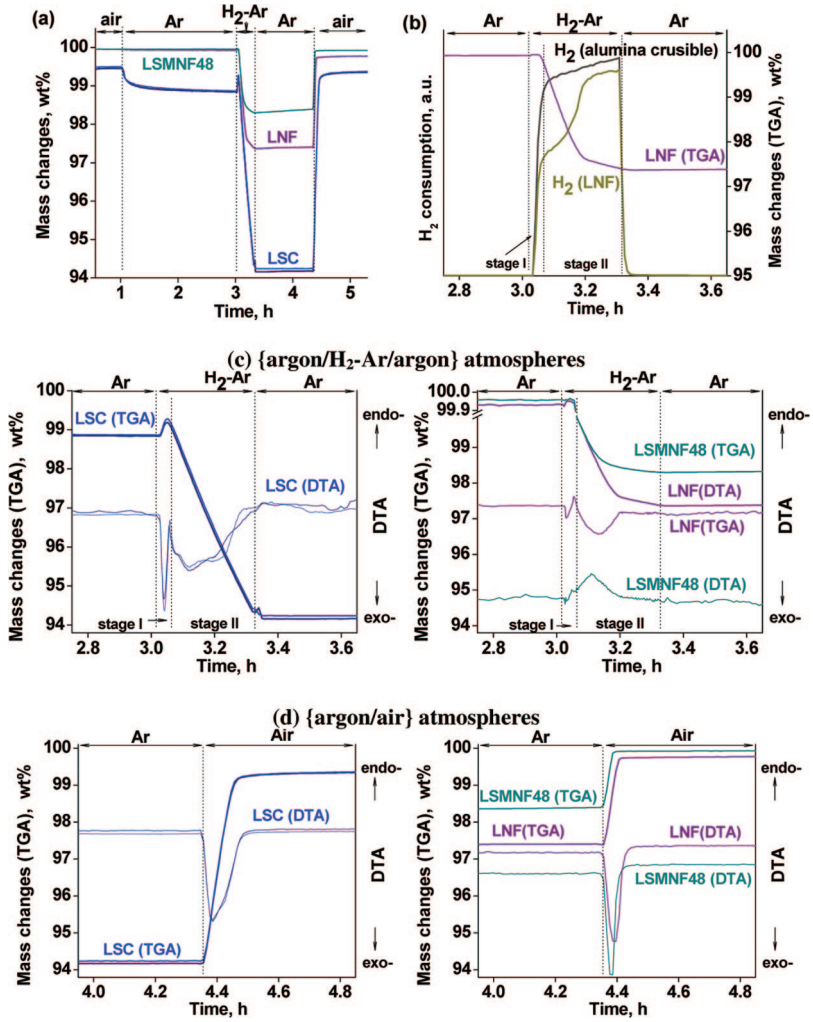

Figure 2. Reduction/reoxidation cycle at 800 °C for LNF, LSMNF48, and LSC after subtraction of the corrections (TGA and DTA): (a) mass change during exposure to different atmospheres, (b) hydrogen consumption in chamber with LNF powder and over an alumina crucible without sample, (c) detail of mass change and DTA under {argon/H_2−Ar/argon} atmospheres, and (d) detail of mass change and DTA under {argon/air} atmospheres.

Table 2. Comparison of BET Surface Area of Powders, Flow Rate of H_2−Ar and Weight Change during Stages I and II at 800 °C

		content of elements in the B sublattice				stage I:	stage II		
composition	[a]abbreviation	Mn	Ni	BET surface area, m^2/g	H_2−Ar gas flow rate, mL/min	weight gain,[b] wt % ± 0.005	weight loss,[b] wt % ± 0.005	change in oxygen content per formula unit, $\Delta(3 \pm \delta)$	change in the average oxidation state of cations in the B sublattice, Δz
LSM	LSM-15	1		0.85 ± 0.04	15	0.025	−0.83	−0.12	−0.24
LSC	LSC-15P			pellet (92% density)	15	0.35			
	LSC-15			1.98 ± 0.09	15	0.36[c]			
	LSC-15H			11.68 ± 0.04	15	0.40			
LNF	LNF-06P		0.6	pellet (93% density)	6	0.01	−2.31	−0.34	−0.68
	LNF-06		0.6	0.27 ± 0.02	6	0.03	−2.26	−0.33	−0.66
	LNF-15		0.6	0.27 ± 0.02	15	0.02	−2.24	−0.33	−0.66
	LNF-32		0.6	0.27 ± 0.02	32	0	−2.31	−0.34	−0.68
	LNF-32H		0.6	4.61 ± 0.06	32	0	−2.56	−0.38	−0.76
	LNF-15vH		0.6	14.13 ± 0.05	15	0.03	−2.69	−0.40	−0.80
LSMNF90	LSMNF90−15	0.1	0.54	3.26 ± 0.20	15	0.03	−2.08	−0.31	−0.62
LSMNF80	LSMNF80−15	0.2	0.48	3.20 ± 0.27	15	0.03	−1.88	−0.28	−0.56
LSMNF48	LSMNF48−15	0.52	0.288	6.18 ± 0.58	15	0.01	−1.28	−0.19	−0.38
	LSMNF48−32	0.52	0.288	6.18 ± 0.58	32	0	−1.52	−0.22	−0.44

[a] The abbreviations presented in Table 2 are used in the text and figures. The abbreviation briefly describes the chemical composition of the materials analyzed, the flow rate of H_2−Ar, and, for some samples, the difference in morphology (in BET surface area or pellet). [b] Data for weight change are presented after subtraction of the buoyancy effect. [c] It was characterized statistically for six samples ±0.02

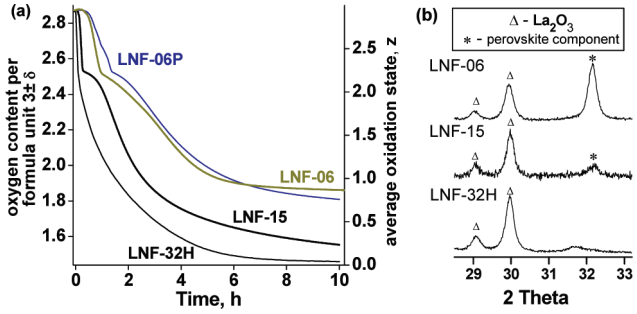

Figure 3. (a) Change in the oxygen content per formula unit and the average oxidation state of cations on the B sublattice of LNF during exposure to H_2−Ar at 800 °C: under different gas flow rates (6, 15, or 32 mL/min) and with different morphology of LNF ("P" stands for pellet, without letter stands for powder with $S_{BET} = 0.27$ m^2/g, "H" stands for powder with $S_{BET} = 4.61$ m^2/g). (b) Detail of XRD patterns of LNF-06, LNF-15, and LNF32H after reduction at 800 °C for 10 h. The samples analyzed are described in more detail in Table 2.

LSMNF90 (Table 2). In the case of LSMNF48, a weight gain was very small and not much higher than the accuracy of TGA (Table 2). This stage lasts up to 0.1 h, and the duration of stage I decreases with the increase in the gas flow rate for LNF powder with the same morphology (LNF-06, LNF-15, and LNF-32) (Table 2 and Figure 3). Notice that special correction TGA runs were carried out at different H_2−Ar flow rates to increase the accuracy of TGA measurements. The comparison of the results presented in Table 2 for powders with different surface area and sintered pellets shows that there is no strict correlation between a weight gain and the size of the BET surface area at this stage.

This could indicate that the chemical nature of the processes contributing to the weight gain at this stage is most important. Probably, there are a number of active sites at the surface, grain boundary, or through volume of powders where chemical sorption of hydrogen could take place. Hydrogen atoms have a small size and could penetrate into the perovskite lattice, forming H^- centers near Me^{n+} cations, as was shown for $LaSrCoO_3H_{0.7}$.[26,27] According to the literature, the formation of 3d metal hydride−oxides was reported only for Co-containing compositions in spite of 3d transition metals (Co, Ni, Fe, Mn, Cr, V, Ti) possessing a wide variety of local environments (stable electronic configurations, oxidation states, and coordination numbers) in solids.[24,26−28] It seems that this new generic class of inorganic materials has not been comprehensively explored so far. In our case, the chemical composition of LSC at the initial stage of exposure to H_2−Ar can be presented as $La_{0.6}Sr_{0.4}CoO_{2.81}H_{0.77}$ (Figure 1). On the other hand, $\{Me^{n+}-O^{k-}\cdots H^{m+}\}$ intermediate complexes in the area closed to the surface or into the bulk of polycrystallites could form at the initial stage of exposure to H_2−Ar, thereby reducing the oxygen lattice. A sharp exothermic peak was observed for LSC and LNF unlike for LSMNF48 within the time period which covers stage I (Figure 2c). It is reproducible and a certain trend was observed: the stronger the weight gain, the larger the exothermic effect. Formation of water is a typically exothermic process. Thermochemistry of complex oxide hydrides has not been explored so far in detail. Further thermochemical investigation of Co- and Ni-containing perovskites should be carried out to give insight into the nature of processes taking place at an earlier stage of exposure to H_2−Ar.

3.2.2. Stage II: Formation of H_2O and Its Release Accompanied by Initial Reduction of Cations in the B Sublattice to Low Oxidation State. Stage II lasted for about 0.2−0.27 h for LNF, LSMNF80, LSMNF90, LSM, and LSMNF48 under H_2−Ar gas flow rate of 15 mL/min. During this stage, a dramatic weight loss was observed for LNF, LSMNF80, LSMNF90, and LSC, whereas that of LSM and LSMNF48 was noticeably lower (Figures 1b and 2a). Notice that a wide exothermic peak was observed for LNF, whereas a wide endothermic peak was revealed for LSMNF48 (Figure 2c). To elucidate the difference, the isothermal experiments were repeated interrupting after 0.2 h of exposure to H_2−Ar,

(26) Hayward, M. A.; Cussen, E. J.; Claridge, J. B.; Bieringer, M.; Rosseinsky, M. J.; Kiely, C. J.; Blundell, S. J.; Marshall, I. M.; Pratt, F. L. *Science* **2002**, *295*, 1882.
(27) Bridges, C. A.; Darling, G. R.; Hayward, M. A.; Rosseinsky, M. J. *J. Am. Chem. Soc.* **2005**, *127*, 5996.
(28) Shannon, R. D. *Acta Crystallogr. A* **1976**, *32*, 751.

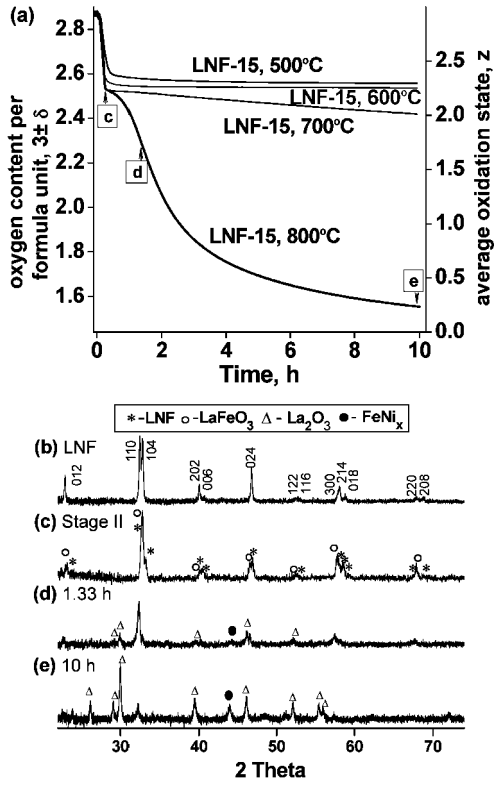

Figure 4. (a) Change in the oxygen content per formula unit in LNF-15 and the average oxidation state of cations in the B sublattice of LNF-15 during isothermal reduction in H_2-Ar (gas flow rate 15 mL/min) at different temperatures (500−800 °C). (b) XRD pattern of LNF powder initially. (c−e) XRD patterns of LNF-15 after different periods of reduction at 800 °C; these periods are marked in part a with the corresponding letters. Part c refers to the middle/end of stage II.

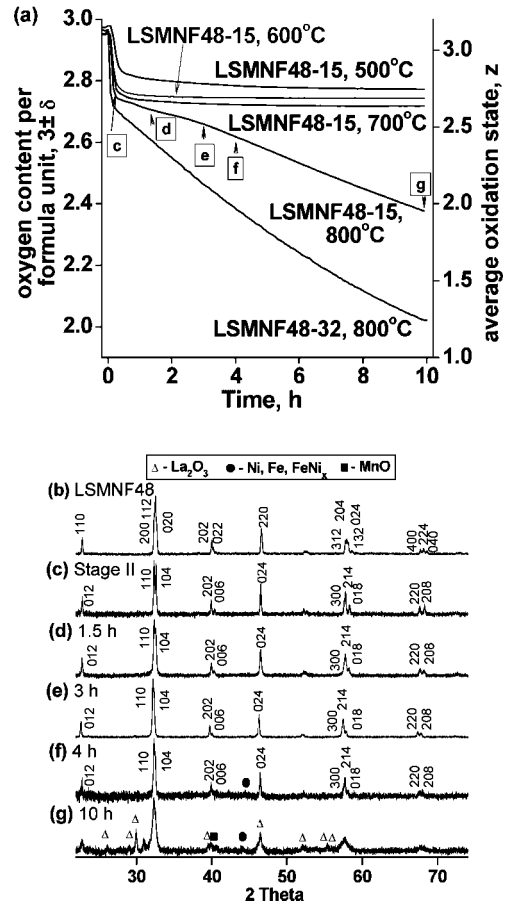

Figure 5. (a) Change in the oxygen content per formula unit and the average oxidation state of cations in the B sublattice of LSMNF48 during isothermal reduction in H_2-Ar at different temperatures and a gas flow rate of 15 mL/min (LSMNF48-15, 500−800 °C) and at 800 °C under high gas flow rate (LSMNF48-32, 32 mL/min). (b) XRD pattern of LSMNF48 powder initially. (c) XRD pattern of LSMNF-15 refers to the middle/end of stage II (after ∼0.2 h of reduction at 800 °C), showing rhombohedral structure. (d−f) XRD patterns of LSMNF48-15 after 1.33−4 h of reduction at 800 °C, showing rhombohedral structure. (g) XRD pattern of LSMNF48-15 after 10 h of reduction at 800 °C.

and both LNF and LSMNF48 samples were cooled down to room temperature in the same atmosphere with a rate of 50 °C/min. A secondary phase ($LaFeO_3$) was observed in the XRD pattern of LNF, whereas the change in symmetry of LSMNF48 from orthorhombic to rhombohedral occurred (Figures 4c and 5c). This suggests that LSMNF48 phase had not degraded severely on initial reduction. This will be discussed further in section 3.2.3. In the case of LSC, several consecutive exothermic peaks were observed in spite of the weight decreasing almost linearly (Figure 2c), indicating a series of fast phase transformations in solid during exposure to H_2-Ar. It seems to be difficult to distinguish stages II and III for LSC, because it completely decomposed to La_2O_3, SrO, and Co within about 1 h (Table 1). This result cannot be explained by the difference in the specific surface area between LSC and others perovskites. LSC possesses, however, the highest anionic conductivity among the perovskites investigated.[29] A high oxygen mobility through the lattice could be important, in particular, in the case of formation of water molecules and their transport from the bulk to the surface of polycrystallites.

Formation of water occurs at this stage. However, water release at 800 °C is the dominant process, leading to a decrease in the weight of the samples investigated. Reduction of cations in the B sublattice to low oxidation state due to charge compensation would be expected. At first glance, the lower the Ni concentration in LNF, LSMNF90, LSMNF80, and LSMNF48, the lower the weight loss (Figure 1b and Table 2). The decrease in the oxygen content per formula unit, $\Delta(3 \pm \delta)$, and the change in the average oxidation state of B cations, Δz, during stage II were evaluated (Table 2). One can see that the decrease in the average oxidation state for LNF, LSMNF90, LSMNF80, and LSMNF48 is slightly higher than expected from the Ni content in the samples if the only process taking place is $Ni^{z+} \rightarrow Ni^{2+}$ (where z could be between 2.8 and 3.0). The discrepancy could be explained by experimental error, but the difference becomes slightly higher with the increase in the gas flow rate and the specific surface area for both LNF and LSMNF48 (Table 2). Reduction of Ni cations to metallic phase was not observed by XRD at 800 °C, although it could occur, in particular, at the surface. It cannot be completely ruled out that partial reduction of manganese cations could also contribute to the weight loss after partial reduction of nickel cations, particularly for LSMNF48 (Table 2). Our observations are in accord with results reported in the literature for $LaBO_3$ perovskites (B = Ni, Mn, Fe).[1] $LaNiO_{3-\delta}$ starts decomposing at 1000 °C

(29) Teraoka, Y.; Zhang, H. M.; Okamoto, K.; Yamazoe, N. *Mater. Res. Bull.* **1988**, *23*, 51.

and $P(O_2) \sim 0.25$ atm to La_2NiO_4 and NiO followed by final decomposition to La_2O_3 and Ni at $P(O_2) \sim 10^{-12}-10^{-13}$ atm. $LaMnO_3$ and $LaFeO_3$ decompose at lower oxygen partial pressure $P(O_2) \sim 10^{-15}$ and $\sim 10-10^{-17}$ atm, respectively.[1]

The defect equilibrium around $\{Me^{n+}-O\cdots H^{m+}\}$ units could be described by means of two simultaneous processes: water formation (reaction 1) and reduction of B cations (reaction 2). The defect equilibrium equation and corresponding equilibrium constant are expressed as

Reaction 1 (R1)

$$H_2 + \frac{1}{2}O_2 = H_2O \tag{5}$$

$$K_{R1} = [H_2O]/([H_2][O_2]^{1/2}) \tag{6}$$

Reaction 2 (R2)

$$2Me^X_{Me} + O^X_O = \frac{1}{2}O_2 + 2Me'_{Me} + V_O^{\bullet\bullet} \tag{7}$$

$$K_{R2} = ([Me'_{Me}]^2[O_2]^{1/2}[V_O^{\bullet\bullet}])/([Me^X_{Me}]^2[O^X_O]) \tag{8}$$

The summary equation and the corresponding equilibrium constant (K_{SUM}) are given as

$$2Me^X_{Me} + O^X_O + H_2 = 2Me'_{Me} + V_O^{\bullet\bullet} + H_2O \tag{9}$$

$$K_{SUM} = ([Me'_{Me}]^2[H_2O][V_O^{\bullet\bullet}])/([Me^X_{Me}]^2[H_2][O^X_O]) \tag{10}$$

The reaction rate for the above-described processes can be written as

$$d([Me'_{Me}]^2[H_2O][V_O^{\bullet\bullet}])/d\tau = k_{12(T)}[Me^X_{Me}]^2[H_2][O^X_O] \tag{11}$$

where k_{12} is the reaction rate constant. One can conclude from eq 11 that the higher the hydrogen concentration, the faster the formation of water and the reduction of cations, i.e. greater weight loss or less oxygen content per formula unit should be observed within a shorter time period. This is in good agreement with the fact that the duration of stage II at 800 °C for LNF powder ($S_{BET} = 0.27$ m^2/g) increased on decreasing the gas flow rate (Figure 3a) (LNF-06 and LNF-15). However, the weight loss of LNF powder ($S_{BET} = 0.27$ m^2/g) measured under different H_2-Ar gas flow rates (6, 15, and 32 mL/min) and of LNF with different morphology (powders with $S_{BET} = 4.61$ and 14.13 m^2/g as well as pellet) after stage II was comparable and amounted to about −2.24 to −2.69 wt %, in spite of the increase in the gas flow rate and the enormous difference in the surface area (LNF-06P, LNF-15, LNF-32H, and LNF-15vH) (Table 2). Notice, that weight loss at this stage slightly varies with temperature (500−800 °C) for both LNF and LSMNF48 (Figures 4a and 5a). One can finally assume that initial reduction (or water formation as the main product) takes place not only on the surface of grains or in pores but also in the bulk of polycrystallites near cations with the highest "reduction activity".

3.2.3. Stage III: Formation of H_2O and Its Release Accompanied by Complete Reduction and Decomposition of Perovskites. The comparison of the weight loss curves for LNF, LSMNF90, LSMNF80, and LSMNF48 (Figure 1b) indicates that A-site- and B-site-substituted complex perovskites reduce more slowly during stage III as compared to LNF. The higher the Sr and Mn concentration in perovskites, the less the oxygen loss was at 800 °C. All these perovskites are A-site-deficient and the degree of deficiency decreases from LNF (0.05) to LSMNF48 (0.024). Further, we would like to discuss the effect of temperature, gas flow rate, and surface area on the complete reduction of LNF and LSMNF48. To study phase or structural transformations in solid at 800 °C, TGA measurements were interrupted after certain time periods and samples were analyzed by XRD and HRTEM.

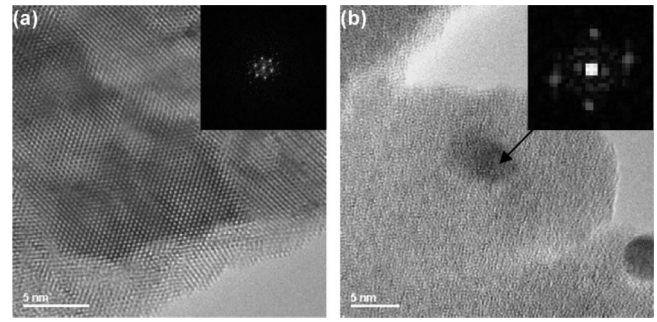

Figure 6. TEM images of LNF-15 after 1.33 h of exposure to H_2-Ar at 800 °C: (a) crystalline phase and (b) amorphous phase with one- and two-dimensional inclusions of metallic phase with corresponding diffraction patterns.

LNF. The oxygen content in LNF-15 ($S_{BET} = 0.27$ m^2/g) was nearly constant after stage II over a period of 10 h in a temperature range between 500 and 700 °C (Figure 4a). According to XRD, LNF and $LaFeO_3$ were both present, even after 10 h of reduction. At 800 °C only a mixture of LNF and $LaFeO_3$ was revealed in the powder after exposure for 0.2 h to H_2-Ar (Figure 4c). The oxygen content in the sample continuously decreased during further exposure at 800 °C (Figure 4a) and was accompanied by further phase transformations. After 1.33 h of reduction, z was slightly less than 2. According to XRD, La_2O_3 and metallic phase were formed (Figure 4d). TEM investigation carried out on this sample showed that an amorphous phase exists in the volume of powder in addition to crystalline phase, probably with hexagonal structure (d-spacings defined from the TEM diffraction patterns are very close to those for La_2O_3) (Figure 6). Small inclusions (~5 nm in diameter) with one- or two-dimensional structures were revealed inside and on the edge of the amorphous phase. These inclusions could represent metallic phase. They were randomly distributed through the sample. Figure 7 illustrates phase distribution at the nanoscale after 4 h of exposure of LNF-15 to H_2-Ar. Three regions can be distinguished within around 10 nm: (i) the crystalline phase, probably with hexagonal structure [d-spacings defined from the TEM diffraction patterns are very close to those for $La(OH)_3$]; (ii) a phase with one-dimensional structure; and (iii) the region between them with unclear structure. Region iii could represent either a reaction zone or a contact area between products of reduction. XRD analysis confirmed that a nearly complete decomposition of LNF to La_2O_3 and $FeNi_x$ intermetallide occurred after 10 h exposure to H_2-Ar

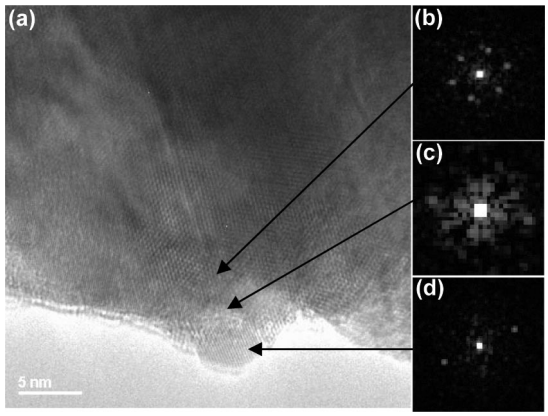

Figure 7. TEM image of LNF-15 after 4 h of exposure to H_2-Ar at 800 °C (a) and diffraction patterns of different areas: (b) crystalline phase with two-dimensional structure, (c) crystalline phase with one-dimensional structure, (d) area between two crystalline phases with unclear structure.

at 800 °C (Table 1 and Figure 4e). The average oxidation state of B cations was almost "0" (Figure 4a, LNF-15). A wide peak relating to $FeNi_x$ phase (44−45° 2Θ) verifies the nanosized metallic particles observed by TEM (Figures 4e, 6, and 7). In addition, a lot of nanoparticles separated from crystalline or amorphous phases were revealed during TEM investigation, indicating poor adherence between products of reduction.

$La(OH)_3$ was observed in the XRD pattern of LNF-15 after 10 h of exposure to H_2-Ar at 800 °C if the sample was cooled down to room temperature at a rate of 5 °C/min (instead of 50 °C/min, as had been done previously), indicating the possibility of $La(OH)_3$ formation during the slow cooling of powders containing large amounts of La_2O_3 as one of the products of reduction. However, TEM investigation indicates the existence of $La(OH)_3$ in LNF-15 reduced for 4 h at 800 °C that was cooled down to room temperature at a rate of 50 °C/min. Notice that $La(OH)_3$ formation was not observed in the XRD pattern of this sample. It means that $La(OH)_3$ could form at high temperature and not only during the slow cooling stage. However, it would be difficult to detect $La(OH)_3$ by XRD, if it forms on the surface of grains in small quantity or as a thin/amorphous layer. In general, the water desorption is a temperature-activated process. According to the literature, $La(OH)_3$ finally decomposed to La_2O_3 and H_2O in the temperature range of 670−810 °C (in air) and at about 600 °C (in vacuum).[30,31] Stabilization of $La(OH)_3$ phase in humidified hydrogen-containing atmosphere seems to be reasonable.

It seems that complete reduction of LNF would be faster if the gas flow rate and specific surface area are increased simultaneously. This can be illustrated by TGA experiments with LNF with different morphology reduced under different H_2-Ar flow rates (6, 15, and 32 mL/min) (Figure 3a). Figure 3b illustrates the difference in the XRD patterns of LNF-06, LNF-15, and LNF-32H after reduction at 800 °C for 10 h. LNF-06 ($S_{BET} = 0.27$ m^2/g) and LNF-06P (pellet) (Table 2) tested under a low gas flow rate (6 mL/min) did not completely reduce within 10 h. The average oxidation state of B cations in LNF-06 and LNF-06P amounts to about 1 (Figure 3a), and the strongest diffraction peak characterizing a perovskite component is clearly observed in the XRD pattern of LNF-06 (Figure 3b). The intensity of the main diffraction peak characterizing a perovskite constituent in LNF-15 is less, but it still can be distinguished (Figure 3b). The complete reduction was observed for LNF-32H ($S_{BET} = 4.61$ m^2/g and gas flow rate of 32 mL/min) within the same time period (Figure 3a,b). Under a low H_2-Ar gas flow rate, probably Fe cations only at the surface of LNF particles or near surface are involved in the reduction processes, whereas Fe cations in cores of grains remain nonreduced or became partially reduced. The average oxidation state of cations in LNF-06 and LNF-06P is about 0.8 after 10 h of exposure to H_2-Ar. LNF contains 40% Fe cations on the B sites. One may assume that the average oxidation state of Fe is close to 2+.

LSMNF48. The oxygen content in LSMNF48, like for LNF, was nearly constant after stage II for 10 h in a temperature range of 500−700 °C (Figure 5a). In contrast to LNF, however, a change in symmetry of LSMNF48 from orthorhombic to rhombohedral structure was observed. The phase with rhombohedral structure was also revealed after exposure to H_2-Ar for 0.2 h at 800 °C (Figure 5c). It means that the phase transformation takes place in a temperature range of 500−800 °C within 0.2 h of initial exposure to H_2-Ar atmosphere. The structural transition could be associated with the reversible red−ox character of $Ni^{n+} \rightarrow Ni^{2+}$ and $Ni^{2+} \rightarrow Ni^{n+}$ couples. On the other hand, this can be represented as a formation of a new intermediate phase that seems to be stable for a relatively long time period at intermediate temperatures in H_2-Ar. The tolerance factor evaluated for the intermediate phase after stage II at 800 °C amounts to 0.90, which is less compared to that for LSMNF48 before reduction (Table 1). During further exposure to H_2-Ar at 800 °C, the oxygen content in LSMNF48 gradually decreased (Figure 5a). After 3 h of reduction, the XRD pattern of the composition remains the same beside the main peak (Figure 5e). There is no clearly splitting of the main peak. However, two diffraction lines could be distinguished through the deconvolution peak procedure, and the whole XRD pattern could be assigned a rhombohedral symmetry. Figure 8 illustrates variation in the room temperature lattice parameters, the unit cell volume, and the tolerance factor for the intermediate phase with rhombohedral symmetry. After exposure for 10 h in H_2-Ar at intermediate temperatures (500−700 °C), the *a* parameter remained almost the same and the *c* parameter slightly increased. However, both *a* and *c* parameters essentially increased after exposure for 3 h at 800 °C (Figure 8b). After 4 h both *a* and *c* parameters remained the same as after 3 h (Figure 5e,f). However, a very small peak in the range of 44−45° 2Θ, which probably belongs to metallic phases, appeared in the XRD pattern, despite all the other peaks remaining the same (Figure 5f). This result indicates that the expansion in both the *a*−*b* plane and along the *c* direction (three-dimension expansion) could lead to destruction of the rhombohedral structure and decomposition of perovskites.

(30) Ozawa, M.; Onoe, R.; Kato, H. *J. Alloys Compd.* **2006**, *408−412*, 556.
(31) Kabashima, H.; Katou, T.; Hattori, H. *Appl. Catal., A* **2001**, *214*, 121.

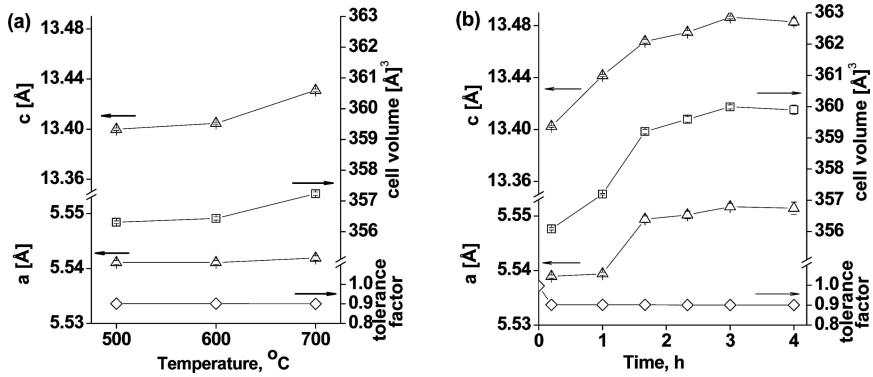

Figure 8. Room temperature lattice parameters, unit cell volume, and tolerance factor of LSMNF48-15 with rhombohedral symmetry after exposure to H_2−Ar (gas flow rate 15 mL/min) (a) for 10 h at different temperatures (500−700 °C) and (b) at 800 °C after different time periods. The room temperature lattice parameters are presented in hexagonal setting.

Notice that the tolerance factor evaluated for intermediate phase with rhombohedral structure after reduction at different temperatures and after different time periods at 800 °C was constant, Figure 8. After 10 h of exposure to H_2−Ar at 800 °C, in addition to metallic phases, peaks of manganese and lanthanum oxides appeared in the XRD pattern, indicating the destruction of rhombohedral structure (Figure 5g).

4. Conclusions

Different phenomena can in general occur during exposure of perovskites to hydrogen-containing atmosphere: sorption and dissociation of hydrogen, formation of $\{Me^{n+}-O\cdots H^{m+}\}$ intermediate complexes initially at the surface of polycrystallites, migration of hydrogen atoms from the surface into bulk of polycrystallites, water formation from intermediate complexes at the surface and in the bulk, Me^{n+} reduction cations due to charge compensation, transport of H_2O molecules from bulk to surface, and H_2O release from the grain's surface or pores. The results obtained in the present study for $A_{1-x}A'_xB_{1-y-z}B'_yB''_zO_{3\pm\delta}$ perovskites (A, A′ = La, Sr and B, B′, B″ = Ni, Mn, Fe, Co) indicate that at the initial stage of exposure to hydrogen-containing atmosphere formation of H^- centers near Me^{n+} cations might take place in addition to formation of $\{Me^{n+}-O^{k-}\cdots H^{m+}\}$ complexes. They both could form not only at the surface but also in the bulk of polycrystallites near cations with the highest "reduction activity". Alternatively, water formed from intermediate complexes could incorporate into the initial structure. It was noticed that initial reduction (or water formation as the main product) takes place not only on the surface of grains or pores but also in the bulk of polycrystallites. Water mobility in the bulk of perovskites is another aspect. The lattice oxygen could also be mobile because of the existence of the anionic vacancies, like in LSC, which permit the oxygen transport from the bulk to the surface and contribute additionally to the water formation and its transport from bulk to surface. This is important for the understanding of the correlation between the defect structure and the thermochemical stability. Finally, these could be accompanied by phase and structural transformations in solid phase. A scheme of phase and structural transformations occurring in $A_{1-x}A'_xB_{1-y-z}B'_yB''_zO_{3\pm\delta}$ perovskites during their exposure to H_2−Ar atmosphere is presented in Figure 9.

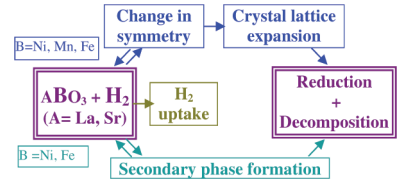

Figure 9. Summary of processes taking place during exposure of perovskites to hydrogen-containing atmosphere.

A small weight gain occurs at the initial stage of exposure of complex perovskites $A_{1-x}A'_xB_{1-y-z}B'_yB''_zO_{3\pm\delta}$ to H_2−Ar (under a gas flow rate of 15 mL/min and lower) at 800 °C. It was also shown that the weight gain can not be simply explained by the size of the specific surface area. This might indicate direct sorption of hydrogen into the lattice. On the other hand, the oxide lattice could reduce to form water, and then, the evolved water is reincorporated into the lattice to give a small gain in weight.

A sharp weight loss was observed for all samples in a temperature range between 500 and 800 °C during further exposure to H_2−Ar. The oxide lattice of perovskite at this stage is also reduced, forming water. This is accompanied by desorption of H_2O and the appearing of free electrons. Due to the charge compensation, reduction of cations in the B sublattice takes place. A sharp weight loss observed at this stage was nearly proportional to the nickel content in $La_{1-x}Sr_xMn_{1-y-z}Ni_yFe_zO_{3\pm\delta}$. It could be attributed to both surface and bulk Ni reduction, if the process $Ni^{n+} \rightarrow Ni^{2+}$ mainly takes place. Perovskites will allow some loss of oxygen, retaining their initial structure. After reaching a certain percentage of oxygen deficiency, which seems to be relatively low, they undergo structural transformations or start decomposing. In the case of LSMNF48, the transformation from orthorhombic to rhombohedral symmetry takes place in a range of oxygen deficiency $2.75 \leq (3 \pm \delta) \leq 2.90$. Further, the rate of processes taking place will be controlled by kinetic factors.

Another important fact is that during long-term exposure in H_2−Ar atmosphere in a temperature range of 500−700 °C the weight of LNF and LSMNF48 perovskite was nearly constant, in spite of the variation in Sr, Ni, and Mn concentration in the A and B sublattices as well as the difference in the phase compositions observed by XRD. On the other hand, both compositions contain lanthanum, which

exhibits strong hydroscopic properties. They also show lower ionic conductivity compared to LSC. Fast formation of H_2O at the initial stage of exposure to H_2-Ar could lead to the appearing of $La(OH)_3$ in the form of a thin layer at the surface of grains and as a fine dispersion randomly distributed through the bulk of perovskites. This could dramatically suppress the hydrogen sorption at the surface as well as oxygen, H_2O, or $(OH)^-$ mobility in the bulk. Decomposition of $La(OH)_3$ is expected at high temperature, since water desorption is a temperature-activated process. This is probably one of the reasons why perovskites kinetically reduce faster at a temperature higher than 700 °C.

In the long term, the perovskite containing three transition elements in the B sublattice and Sr in the A sublattice is kinetically more stable under reducing conditions at intermediate temperatures. The chemical nature of both A and B elements in the multisubstituted perovskites are of great importance, since their interaction could determine the local surroundings in the crystal lattice, the mobility of different species [hydrogen, H_2O, $(OH)^-$, oxygen], and, as a consequence, the stability of $A_{1-x}A'_xB_{1-y-z}B'_yB''_zO_{3\pm\delta}$ perovskite in an aggressive hydrogen-containing environment.

Acknowledgment. We thank Mr. R. Blackley for HRTEM analysis and Mrs. S. Williamson for BET analysis, as well as EPSRC for financial support.

Supporting Information Available: Corrections and original TGA−DTA data for the reduction/reoxidation cycle. This material is available free of charge via the Internet at http://pubs.acs.org.

CM802996P